Journal of Modern Optics
Publication details, including instructions for authors and subscription information:
http://www.tandfonline.com/loi/tmop20

Characteristics of single-mode InGaAs sub-monolayer quantum-dot photonic-crystal VCSELs emitting in the 990 nm range

Hung-Pin D. Yang [a], I.-Chen Hsu [b], Fang-I. Lai [b], Gray Lin [a], Ru-Shang Hsiao [a], Hao-Chung Kuo [b] & Jim Y. Chi [a]

[a] Nanophotonic Center, Industrial Technology Research Institute, Hsinchu, Taiwan

[b] Institute of Electro-Optical Engineering, National Chiao Tung University, Hsinchu, Taiwan

Published online: 11 Apr 2008.

To cite this article: Hung-Pin D. Yang, I.-Chen Hsu, Fang-I. Lai, Gray Lin, Ru-Shang Hsiao, Hao-Chung Kuo & Jim Y. Chi (2008) Characteristics of single-mode InGaAs sub-monolayer quantum-dot photonic-crystal VCSELs emitting in the 990 nm range, Journal of Modern Optics, 55:6, 1013-1021, DOI: 10.1080/09500340701576288

To link to this article: http://dx.doi.org/10.1080/09500340701576288

Journal of Modern Optics
Vol. 55, No. 6, 20 March 2008, 1013–1021

Taylor & Francis
Taylor & Francis Group

Characteristics of single-mode InGaAs sub-monolayer quantum-dot photonic-crystal VCSELs emitting in the 990 nm range

Hung-Pin D. Yang[a]*, I.-Chen Hsu[b], Fang-I. Lai[b], Gray Lin[a], Ru-Shang Hsiao[a], Hao-Chung Kuo[b] and Jim Y. Chi[a]

[a]*Nanophotonic Center, Industrial Technology Research Institute, Hsinchu, Taiwan;* [b]*Institute of Electro-Optical Engineering, National Chiao Tung University, Hsinchu, Taiwan*

(*Received 28 January 2007; final version received 13 July 2007*)

We have made InGaAs sub-monolayer (SML) quantum dot photonic crystal vertical-cavity surface-emitting lasers (QD PhC-VCSELs) for fiber-optic applications. The active region of the device contains three InGaAs SML QD layers. Each of the InGaAs SML QD layer is formed by alternate deposition of InAs (<1 ML) and GaAs. Single fundamental mode CW output power of 3.8 mW at 28 mA has been achieved in the 990 nm range, with a threshold current of 0.9 mA. Side-mode suppression ratio (SMSR) larger than 35 dB has been demonstrated over the entire current operation range. Near-field images of the PhC-VCSELs were also measured and studied.

Keywords: InGaAs; photonic-crystal; sub-monolayer; quantum-dot; VCSEL

1. Introduction

Vertical-cavity surface-emitting lasers (VCSELs) have attracted a lot of attention in recent years. Single-mode VCSELs are necessary for a number of applications, including high-speed laser printing, optical storage and long-wavelength telecommunications. Small oxide aperture VCSELs below about 4 μm diameter operate in the fundamental transverse mode. However, the large resistance inherited from the small aperture limits the modulation bandwidth and degrades the high-speed performance. The lifetime of the oxide VCSEL also decreases proportionally to the diameter of the oxide aperture, even when the device is operated at a reduced current [1]. When the aperture diameter is increased to obtain higher output power, however, multiple higher-order transverse modes oscillate, causing increased noise, a broadened spectrum, and a strong increase of the far-field angle. Techniques used to solve the problem include the increase of higher-order mode loss by surface-relief etching [2], hybrid oxide-implanted VCSELs [3,4] and two-dimensional triangular holey structure [5]. Recently, two-dimensional photonic crystal (2-D PhC) structure formed on the VCSEL surface has been used as a control

*Corresponding author. Email: hpyang@itri.org.tw

ISSN 0950–0340 print/ISSN 1362–3044 online

DOI: 10.1080/09500340701576288
http://www.informaworld.com

method of transverse modes. Single-mode output was realized from larger aperture photonic crystal VCSELs (PhC-VCSELs) [6, 7]. However, those PhC-VCSELs exhibit relatively high threshold currents (I_{th}) due to large oxide confined apertures. For long-wavelength applications, InAs quantum-dot (QD) VCSELs [8] and QD PhC-VCSELs [9] achieved laser emission at 1300 nm. For shorter wavelength emission, InGaAs/GaAs sub-monolayer (SML) quantum dot (QD), embedded in a GaAs matrix shows luminescence peaks and high power lasing performance in the 0.92–1 μm range [10].

Recently single-mode InGaAs SML QD VCSELs with room-temperature output power as high as 4 mW have been demonstrated [11]. However, single-mode operation of the InGaAs SML QD VCSEL with PhC is still yet to be realized. In this paper, we report our results on the InGaAs QD PhC-VCSELs in the 990 nm range. Single-transverse-mode operation with very high side-mode suppression ratio (SMSR) is demonstrated for the first time. The beam profiles of the PhC-VCSELs were measured and analyzed.

2. Epitaxial growth and device fabrication

The epitaxial layers of the InGaAs SML QD PhC-VCSEL wafers were grown on 3 inch n^+-GaAs (001) substrates by molecular beam epitaxy (MBE) in a Riber 49 chamber. The bottom distributed Bragg reflector (DBR) consists of a 33-pair n-type (Si-doped) quarter-wave stack ($\lambda/4$) of $Al_{0.9}Ga_{0.1}As$/GaAs. The top DBR consists of 20-period p-type (carbon-doped) $Al_{0.9}Ga_{0.1}As$/GaAs quarter-wave stack. Above that, is a heavily doped p-type GaAs contact layer. The undoped 1λ-cavity contains three InGaAs SML QD layers, separated by GaAs barrier layers. Each of the InGaAs SML QD layers is formed by alternate deposition of InAs (<1 ML) and GaAs. A 20 nm thick AlAs oxidation layer is placed within the p-type $Al_{0.9}Ga_{0.1}$ as confinement layer. Firstly, mesas with diameters varying from 50 to 68 μm were defined by reactive ion etch (RIE). The p-ohmic contact ring with an inner diameter 4 μm larger than the oxide aperture was formed on the top of the p-contact layer. The AlAs layer within the $Al_{0.9}Ga_{0.1}As$ confinement layer was selectively oxidized to AlO_x. The oxidation depth was about 15 to 16 μm toward the center from the mesa edge so that the resulting oxide aperture varied from 18 to 38 μm in diameter. The oxide aperture was introduced in minimum of optical field in order to reduce the lateral optical loss and the leakage current. The n-ohmic contact was formed at the bottom of the n^+-GaAs substrate. After that, triangular lattice patterns of photonic crystal with a single-point defect in the center were defined within the p-contact ring using photo-lithography and etched through the p-type DBR using RIE. The lateral index around a single defect can be controlled by the hole radius (r)-to-lattice constant (a) ratio and etching depth [6]. This ratio (r/a) is 0.25; the lattice constant a is 5 μm in the PhC-VCSEL and the etching depth of the holes is about 16-pair thick into the 20-pair top DBR layer. The normalized lattice constant (a/λ) is 5.05 (for $\lambda = 990$ nm). The ratio (r/a) of 0.25 is chosen for better optical confinement and ensuring single mode operation [12]. The designed lattice parameters also provide suitable conduction paths (~2.5 μm) for the injection current to flow between vertically etched PhC holes, and then flow toward the central single-point defect area for laser emission. The refractive index of the PhC hole

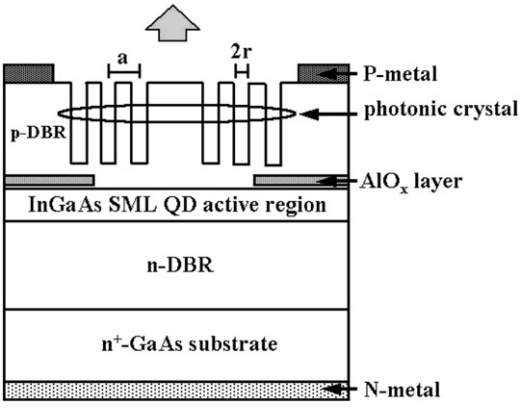

Figure 1. Schematic of InGaAs SML QD PhC-VCSEL. The hole etching depth of the PhC is 16-pair out of the 20-pair top DBR been etched off.

area is reduced, as compared to that of the central un-etched area. The device structure is shown in Figure 1. By using two types of apertures in this device, we decouple the effects of the current confinement from the optical confinement. The selectively oxidized AlO_x layer is used to confine the current flow, while the single-point defect (approximately $\geq$10 μm in diameter) photonic-crystal structure is used to confine the optical mode. In order to clarify the effect of the photonic-crystal index-guiding layer, an oxide-confined VCSEL (oxide aperture is approximately 18 to 20 μm in diameter without PhC) was also fabricated for comparison.

3. Results and discussions

The continuous-wave (CW) light–current–voltage (*L–I–V*) output of the InGaAs SML QD VCSEL without photonic crystal (PhC) is shown is Figure 2(*a*). The oxide aperture of the device is approximately 20 μm in diameter. The maximum output power is 12.2 mW at 30 mA, with a threshold current (I_{th}) of approximately 1 to 2 mA. The slope efficiency is 0.45 to 0.65 W A^{-1} from 1.5 to 16 mA. The device shows multiple transverse mode characteristics. The differential series resistance of the VCSEL without PhC is approximately 10 Ω at 12 mA. The mesa of the VCSEL is 50 μm in diameter. Figure 2(*b*) shows CW *L–I–V* output of the PhC-VCSEL. The near-field image of the PhC-VCSEL operated at 4 mA is also shown (inset). The I_{th} of the PhC-VCSEL is 0.9 mA, with an oxide aperture of approximately 18 μm in diameter. The PhC-VCSEL emits 3.8 mW maximum power at 28 mA and exhibits single mode operation throughout the current range of operation. This is one of the highest output powers achieved for PhC-VCSELs. The slope efficiency is approximately 0.15 to 0.22 W A^{-1} from 3 to 15 mA. The near-field image of the lasing output remains as the fundamental TEM_{00} mode at the center of the PhC structure throughout the current operating range. From the near-field image, laser emission from the six photonic crystal holes surrounding the single-point defect area was also observed. This laser emission from the photonic crystal holes corresponds to an

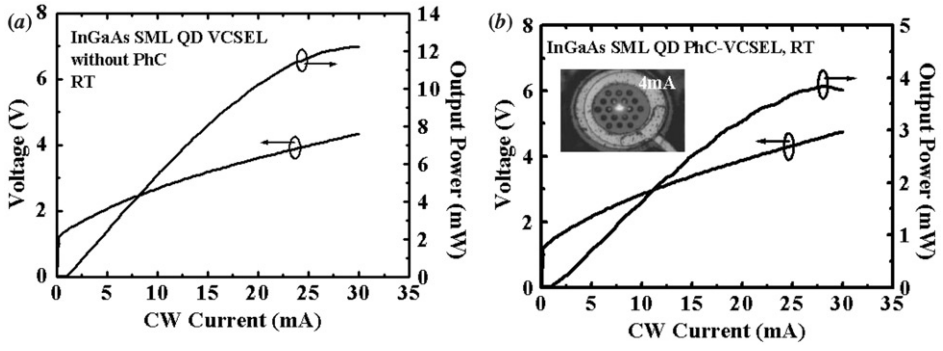

Figure 2. CW *L–I–V* characteristics of the InGaAs SML QD (*a*) VCSEL without PhC. (*b*) PhC-VCSEL. The ratio r/a is 0.25 and the lattice constant a is 5 μm for the PhC-VCSEL. The near-field image of the PhC-VCSEL at 4 mA is shown in the inset. The measurement temperature was room temperature (RT).

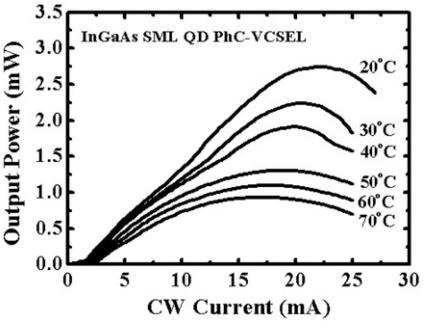

Figure 3. Temperature-dependent *L–I* characteristics of the InGaAs SML QD PhC-VCSEL.

off-axis laser beam deviated from the optic axis perpendicular to the top-emitting surface of the VCSEL. The differential series resistance of the PhC-VCSEL is approximately 125 Ω at 12 mA. The *I–V* characteristics exhibit slightly higher series resistance for the PhC-VCSEL, which should be mainly due to blocking of the current flow in the region by photonic crystal holes. Figure 3 shows the temperature-dependent light–current (*L–I*) characteristics of the PhC-VCSEL. The threshold current increases from 1.3 mA at 20°C to 2.2 mA at 70°C. The maximum output power decreases from 2.7 mW at 20°C to 0.9 mW at 70°C.

Lasing spectra of the PhC-VCSEL is shown in Figure 4(*a*), confirming single-mode operation within overall operation current. The peak lasing wavelengths are 991, 992, and 996 nm at 3, 9, and 20 mA, respectively. The PhC-VCSEL exhibits a SMSR > 35 dB throughout the current range. Figure 4(*b*) shows the current-dependent peak wavelength of the PhC-VCSEL. The peak lasing wavelength increases monotonically with the driving current. For comparison, lasing spectra of the InGaAs SML QD VCSEL without photonic crystal holes shows multiple transverse mode operation as the driving current is increased above I_{th} (Figure 5). The InGaAs SML QD VCSEL without PhC shows multiple transverse mode characteristics with a broader wavelength span.

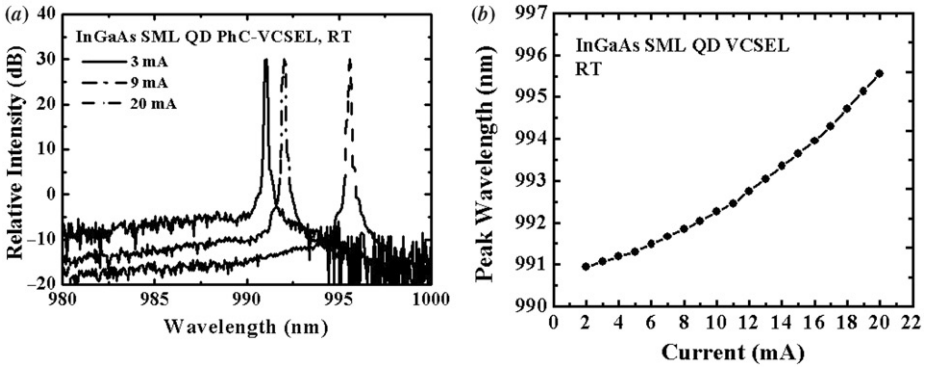

Figure 4. (*a*) Spectra and (*b*) current-dependent peak wavelength of an InGaAs SML QD PhC-VCSEL. The measurement temperature was room temperature.

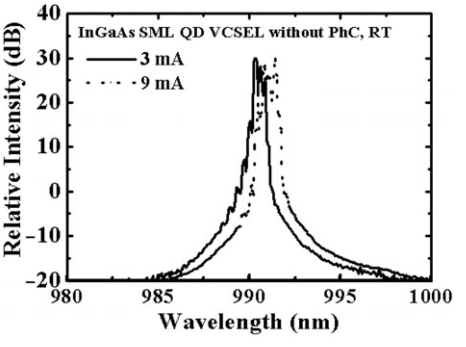

Figure 5. Spectra of an InGaAs SML QD VCSEL without PhC. The measurement temperature was room temperature.

Figure 6(*a*) is the near-field image of the PhC-VCSEL at 10 mA, with light illumination on the devices in order to show the laser emission pattern and the photonic crystal structure simultaneously. The fundamental TEM_{00} laser output is well confined at the center of the single-point defect area. The laser beam emits not only from the single-point defect area at the center of the photonic crystal structure, but also from the six photonic crystal holes nearby. The laser beam intensity increases with increasing biasing current before thermal rollover occurs. The stray laser emission from the photonic crystal holes is believed to be the off-axis laser emission and diffraction within the laser cavity [13]. There is no other laser emission spot observed, indicating that there is no other lasing mode within the device. This off-axis laser emission also contributes to the divergence angle of the laser beam. The reflectance of the remaining p-DBR layers within the photonic crystal hole is significantly reduced due to RIE etch. The portion of the active region below the PhC hole cannot achieve lasing condition because of lower reflectance of the remaining p-type DBR layers. Therefore, the laser emission from the photonic crystal holes must be contributed from off-axis laser

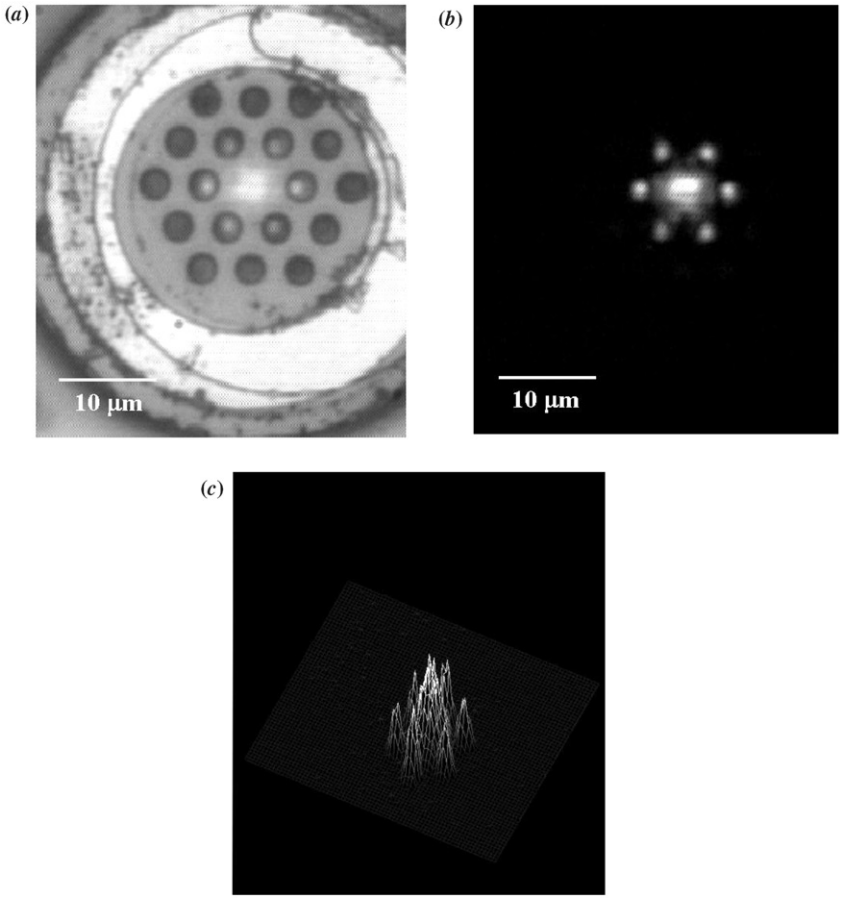

Figure 6. (*a*) Near-field image at 10 mA, (*b*) near-field image at 16 mA without additional light illumination, and (*c*) three-dimensional (3-D) near-field intensity profile at 10 mA of the InGaAs SML QD PhC-VCSEL.

emission and diffraction originated from the TEM_{00} mode at the center. Other stray laser emission was blocked by the high-reflectance top DBR. The measured single-mode spectra in Figure 4 indicate that all the laser emission beams, including those from the photonic crystal holes, are of the same lasing wavelength. The spectral single-mode characteristics of the PhC-VCSEL are not affected by the laser emission from the photonic crystal holes. The near-field image of the PhC-VCSEL at 16 mA is shown in Figure 6(*b*). The near-field image was taken without addition light illumination. The stray laser emission from the six photonic-crystal holes with smaller beam spot sizes was also observed at all current levels. The spot size of the fundamental TEM_{00} mode remains unchanged throughout the current range. The three-dimensional (3-D) near-field intensity profiles at 10 mA are shown in Figure 6(*c*). The height of the intensity profile is the relative intensity of the lasing output at that position. The laser output consists of one TEM_{00} mode emission at the center and six smaller beams with lower intensity.

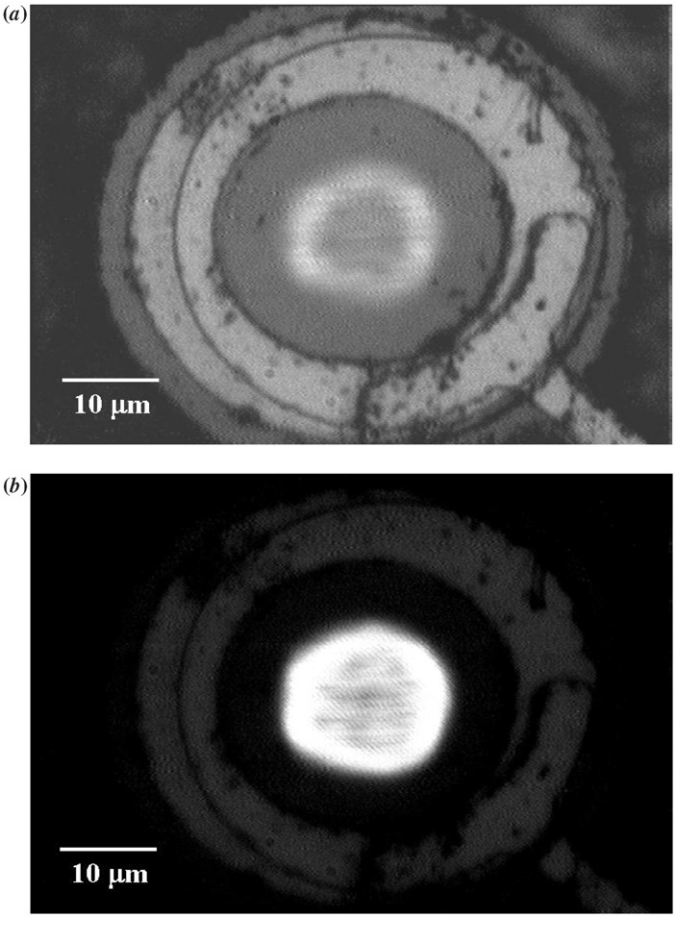

Figure 7. Near-field images of InGaAs SML QD VCSEL without PhC at (*a*) 3 mA and (*b*) 10 mA.

The near-field images of the VCSEL without PhC at 3 and 7 mA are shown in Figure 7. The laser output exhibits a multi-mode beam profile with higher intensity at the periphery. This is mainly because of the current spreading, where the inner diameter of the p-ohmic contact ring is 31 μm. The lasing output of the VCSEL without PhC structure is mainly confined by the AlO_x oxide aperture of the device. The intensity of the laser beam increases with increasing current.

The beam profile results obtained from the far-field beam divergence angle measurement system are shown in Figures 8–10. The divergence angles are the full-width half-maximum (FWHM) of the measured beam profiles in Figures 8 and 9. The beam profiles of the PhC-VCSEL are shown in Figure 8. The beam divergence angle obtained from the beam profile of the device remains to be 6.7° to 6.9°. This very small divergence angle indicates that the laser beam is well confined by the photonic structure of the device. Figure 9 shows the beam profiles of the VCSEL without PhC at 3, 7, and 10 mA. The divergence angle increases with increasing current, from 17.2° at 3 mA to 21.5° at 10 mA.

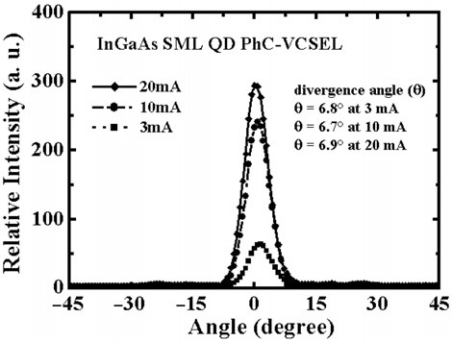

Figure 8. Beam profiles of InGaAs SML QD PhC-VCSEL, measured at 3, 10, and 20 mA.

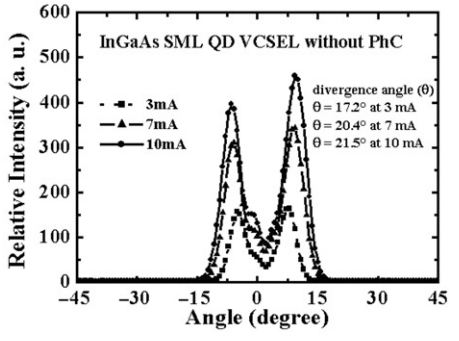

Figure 9. Beam profiles of InGaAs SML QD VCSEL without PhC, measured at 3, 7, and 10 mA.

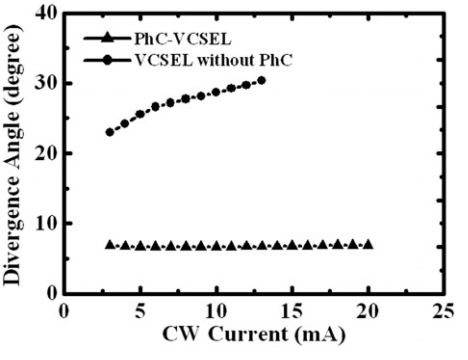

Figure 10. Current-dependent beam divergence angle of the InGaAs SML QD PhC-VCSEL and InGaAs SML QD VCSEL without PhC.

The two laser emission lobes correspond to the annular-shaped laser emission observed by the near-field image in Figure 7. Figure 10 shows the current-dependent divergence angle of the InGaAs SML QD PhC-VCSEL and InGaAs SML QD VCSEL without PhC. For the InGaAs SML QD PhC-VCSEL, the divergence angle remains almost unchanged within 6.7° to 6.9°. For the InGaAs SML QD VCSEL without PhC, the divergence angle increases monotonically with current.

4. Conclusion

We report single-mode InGaAs SML QD PhC-VCSELs with SMSR > 35 dB throughout the operation current range. A maximum single-mode output power of 3.8 mW has been demonstrated. The present results indicate that a VCSEL using an oxide layer for current confinement and photonic crystal for optical confinement is a promising approach to achieve single-mode operation of VCSEL. The beam profile study of the PhC-VCSEL indicates that the laser beam is well confined by the photonic crystal structure of the device.

Acknowledgements

The authors would like to thank Dr A.R. Kovsh of NL Nanosemiconductor GmbH in Germany for providing the InGaAs SML QD-VCSEL epitaxial wafers. The authors would also like to thank Dr N.A. Maleev and Mr S.A. Blokhin of Ioffe Physico-Technical Institute in Russia for useful discussions. This work was supported by the Nanophotonics Project, MOEA.

References

[1] Hawkins, B.M.; Hawthorne III, R.A.; Guenter, J.K.; Tatum, J.A.; Biard, J.R. *Proceedings of the 52nd Electronic Compounds and Technology Conference,* San Diego, CA, May 28–31, 2002, p. 540.
[2] Haglund, A.; Gustavsson, J.S.; Vukusic', J.; Modh, P.; Larsson, A. *IEEE Photon. Technol. Lett.* **2004**, *16*, 368–370.
[3] Hsueh, T.H.; Kuo, H.C.; Lai, F.I.; Laih, L.H.; Wang, S.C. *Electron. Lett.* **2003**, *39*, 1519–1521.
[4] Young, E.W.; Choquette, K.D.; Chuang, S.L.; Geib, K.M.; Fischer, A.J.; Allerman, A.A. *IEEE Photon. Technol. Lett.* **2001**, *13*, 927–929.
[5] Furukawa, A.; Sasaki, S.; Hoshi, M.; Matsuzono, A.; Moritoh, K.; Baba, T. *Appl. Phys. Lett.* **2004**, *85*, 5161–5164.
[6] Yokouchi, N.; Danner, A.J.; Choquette, K.D. *Appl. Phys. Lett.* **2003**, *82*, 1344–1346.
[7] Berkedal, D.; Gregersen, N.; Bischoff, S.; Madsen, M.; Romsted, F.; Oestergarrd, *J. Optical Fiber Communications Conference Proceedings*, 2003, p. 83.
[8] Lott, J.A.; Ledentsov, N.N.; Ustinov, V.M.; Maleev, N.A.; Zhukov, A.E.; Kovsh, A.R.; Maximov, M.V.; Volvovik, B.V.; Alferov, Z.H.I.; Bimberg, D. *Electron. Lett.* **2000**, *36*, 1384–1385.
[9] Yang, H.P.D.; Chang, Y.H.; Lai, F.I.; Yu, H.C.; Hsu, Y.J.; Lin, G.; Hsiao, R.S.; Kuo, H.C.; Wang, S.C.; Chi, J.Y. *Electron. Lett.* **2005**, *41*, 1130–1132.
[10] Mikhrin, S.S.; Zhukov, A.E.; Kovsh, A.R.; Maleev, N.A.; Ustinov, V.M.; Shernyakov, Yu, M.; Soshnikov, I.P.; Livshits, D.A.; Tarasov, I.S.; Bedarev, D.A.; *et al.*, *Semicond. Sci. Technol.* **2000**, *15*, 1061–1064.
[11] Blokhin, S.A.; Maleev, N.A.; Kuzmenkov, A.G.; Shernyakov, Yu.M.; Novikov, I.I.; Gordeev, N.Yu.; Sokolovskii, G.S.; Dudelev, V.V.; Kuchinskii, V.I.; Kulagina, M.M.; *et al.*, *Semiconductors* **2006**, *40*, 615–619.
[12] Yokouchi, N.; Danner, A.J.; Choquette, K.D. *Appl. Phys. Lett.* **2003**, *82*, 3608–3610.
[13] Siegman, A.E. *Lasers*; University Science Books: Mill Valley, CA, 1986; Chapters 1 and 23.